ELSEVIER

International Journal of Mass Spectrometry 185/186/187 (1999) 961–975

International Journal of Mass Spectrometry

Mg^+NO and Mg^+ON: potentially important ionospheric species

Brian C. Hoffman, Henry F. Schaefer III*

Center for Computational Quantum Chemistry, University of Georgia, Athens, GA 30602, USA

Received 16 September 1998; accepted 14 October 1998

Abstract

In order to determine the lowest energy isomer of the $Mg^+ - NO$ complex, self-consistent field (SCF), configuration interaction including all single and double excitations (CISD), coupled cluster singles and doubles (CCSD), and CCSD with perturbatively evaluated triples [CCSD(T)] ab initio electronic structure methods were employed. Equilibrium geometries, relative energies, dipole moments, harmonic vibrational frequencies, and associated infrared (IR) intensities for the lowest triplet and closed-shell singlet structures were determined. At the CCSD(T) level with the largest basis set, triple-ζ plus double polarization augmented with one set of higher angular momentum and one set of diffuse functions (TZ2PF + diff), the global minimum was predicted to be closed shell, $^1A'$ Mg^+NO with equilibrium geometry $r_e(Mg - N) = 2.378$ Å, $r_e(N - O) = 1.147$ Å, and $\theta_e = 122.6°$. At this same level of theory, $^1A'$ Mg^+NO was predicted to lie approximately 14 kcal mol^{-1} below the $Mg^+ + NO$ dissociation asymptote. At levels of theory below CCSD(T), the $^3\Pi$ state of Mg^+NO is erroneously predicted to be the ground state. The dipole moment with respect to the center of mass is predicted to be 4.9 debyes for the $^1A'$ ground state of Mg^+NO. (Int J Mass Spectrom 185/186/187 (1999) 961–975) © 1999 Elsevier Science B.V.

Keywords: Ionospheric species; Electronic structure calculations

1. Introduction

Metallic species detected in the Earth's upper atmosphere, including Na, K, Ca, Mg, and Fe, are produced via thermal ablation of meteors and meteoroids. Iron and magnesium are the most abundant metals present within these cosmic particles, each accounting for approximately 12% by weight [1]. Recently, the simultaneous resonant-scattering detection of neutral Mg and Mg^+ in the thermosphere was achieved using the Arizona Airglow (GLO) instrument placed aboard space shuttle mission STS-53 [2,3]. From the space shuttle data, it was determined that Mg^+ is roughly 34 times more abundant than neutral Mg. These observations prompted McNeil, Lai, and Murad [4] to construct a model for meteoric magnesium in the ionosphere. In their model, charge transfer reactions with cationic species such as O_2^+ and NO^+ are proposed to be one source of Mg^+.

The NO molecule is particularly interesting because it is one of the few abundant neutral diatomic radicals. The unpaired electron in NO is easy to remove, giving NO a relatively low ionization energy (IE) of 9.26 eV compared to 15.58 eV for N_2 and 12.07 eV for O_2. In a charge transfer reaction, the reactant that loses an electron is almost always the one with the lowest IE. Therefore, NO serves as a sink for positive charge in the upper atmosphere, making NO^+ relatively abundant and able to participate in charge

* Corresponding author.

Dedicated to Professor Michael T. Bowers on the occasion of his 60th birthday.

PII S1387-3806(98)14213-6

transfer reactions with neutral metal atoms, one of the few available atmospheric species with lower IEs than NO. The charge transfer reaction between neutral Mg and NO^+ in the ionosphere involves a nonadiabatic jump from the $Mg - NO^+$ potential energy surface (PES) to a lower-lying $Mg^+ - NO$ PES. The energy separation of the $Mg^+ + NO$ and $Mg + NO^+$ asymptotes of these surfaces is 1.6 eV (37.1 kcal mol^{-1}), i.e. the difference between the 7.65 eV IE of Mg and the IE of NO. This research focuses on the determination of the structure and dissociation energy of the lowest energy isomer of the $Mg^+ - NO$ complex with the goal of assisting future investigation into this mechanism of Mg^+ formation.

The Mg^+NO complex was also examined because magnesium containing ion–molecule complexes have been the subject of many recent experimental [5–13] and theoretical [14–24] investigations. Ion–molecule complexes containing metal atoms are of general interest because they provide a model for elucidating the interactions involved in metal–ligand bonding, metal ion solvation, and metal–surface adsorbate reactions. Magnesium complexes have received a large amount of attention, in particular, because the Mg^+ ion is isoelectronic with sodium and possesses a strong $^2S \rightarrow {}^2P$ transition analogous to the sodium D line, making it highly amenable to spectroscopic investigation. The spectroscopy of magnesium ion–molecule complexes is also aided by the natural occurrence of three magnesium isotopes (^{24}Mg, ^{25}Mg, and ^{26}Mg). Furthermore, the magnesium atom is small enough to be treated by high level ab initio electronic structure methods including coupled cluster theory and light enough so that both relativistic and spin–orbit effects are largely negligible. The ability to obtain both theoretical and experimental results for the same complex provides a strong motivation for the study of magnesium complexes.

2. Theoretical approach

The $Mg^+ - NO$ complex is formed via electrostatic interactions, primarily charge–dipole, between the Mg^+ cation (^2S ground state) and the neutral NO radical ($^2\Pi$ ground state). If the Mg^+ cation approaches along the internuclear axis of the NO radical, thereby maintaining $C_{\infty v}$ symmetry, the $Mg^+ +$ NO asymptote may give rise to Mg^+NO and Mg^+ON complexes in $^1\Pi$ and $^3\Pi$ electronic states. Alternately, the Mg^+ cation could approach at an angle to the NO internuclear axis, reducing the overall symmetry to C_s and potentially producing Mg^+NO and Mg^+ON complexes in $^1A'$, $^1A''$, $^3A'$, and $^3A''$ electronic states, as well as in a closed-shell $^1A'$ electronic state. When searching for the lowest energy isomer, however, one probably need not exhaustively consider the open-shell $^1\Pi$, $^1A'$, and $^1A''$ electronic states because according to Hund's rules, the corresponding $^3\Pi$, $^3A'$, and $^3A''$ states should lie lower in energy. Therefore, all possible complexes, with the exception of those in open-shell singlet states, were carefully considered in the present study.

Three basis sets of triple-ζ quality in the valence space were employed in the investigation of Mg^+NO. The basis sets were derived from the McLean–Chandler triple-ζ $(12s9p/6s5p)$ contracted set for magnesium [25] and the Huzinaga–Dunning triple-ζ $(10s6p/5s3p)$ contracted sets for nitrogen and oxygen [26,27]. The smallest basis set, denoted TZP, consisted of the triple-ζ contractions centered on each atom augmented by a set of d-like polarization functions with orbital exponents $\alpha_d(Mg) = 0.20$, $\alpha_d(N) = 0.80$, and $\alpha_d(O) = 0.85$, giving a total of 64 basis functions. The TZP basis set was augmented by the addition of a set of P diffuse functions on magnesium [$\alpha_p(Mg) = 0.01336$] and a set of S and P diffuse functions on nitrogen and oxygen [$\alpha_s(N) = 0.06742$, $\alpha_p(N) = 0.04959$, $\alpha_s(O) = 0.07938$, and $\alpha_p(O) = 0.05840$] to yield the TZP + diff basis set. The largest basis set employed, denoted TZ2PF + diff, consisted of the TZP + diff basis set modified by exchanging single polarization for double [$\alpha_d(Mg) = 0.30$ and 0.10, $\alpha_d(N) = 1.60$ and 0.40, and $\alpha_d(O) = 1.70$ and 0.425] and the addition of a set of f-like higher angular momentum functions on each atom with orbital exponents $\alpha_f(Mg) = 0.25$, $\alpha_f(N) = 1.0$ and $\alpha_f(O) = 1.4$. The TZ2PF + diff basis set contained a total of 111 basis functions. Pure angular momentum $(5d,7f)$ functions were used throughout.

For each of the three basis sets, the closed-shell singlet and open-shell triplet Mg^+NO and Mg^+ON structures were optimized using analytic gradient techniques at the self-consistent field (SCF) [28,29], configuration interaction including all single and double excitations (CISD) [30–33], coupled cluster singles and doubles (CCSD) [34–36], and CCSD with perturbative triples [CCSD(T)] [35,37,38] levels of theory. In all cases, residual internal coordinate gradients were less than 10^{-6} in atomic units. At the CISD level of theory, three core orbitals (Mg, N, and O 1*s*-like) were frozen and the corresponding virtual (Mg, N, and O 1*s**-like) orbitals were deleted. With the largest basis set, TZ2PF + diff, the number of configuration state functions (CSFs) included in the CISD wave functions in C_{2v} symmetry for the $^3\Pi$ structures and C_s for the $^1A'$ structures were 143 468 and 234 232, respectively. With the CCSD and CCSD(T) methods, all of the electrons were correlated and no virtual orbitals were deleted. Harmonic vibrational frequencies and associated infrared (IR) intensities were determined via analytic second derivatives at the SCF [39–41] level of theory and by finite differences of gradients at the CISD, CCSD, and CCSD(T) levels of theory. Dipole moments were determined with respect to the center of mass in all cases. The SCF and CISD calculations were performed using the PSI [42] suite of quantum chemistry programs, whereas all coupled cluster results were obtained using the ACES II [43] ab initio program system.

3. Results and discussion

3.1. Closed-shell $^1A'$ structures of Mg^+NO and Mg^+ON

3.1.1. Electronic structures

The closed-shell $^1A'$ structure of the Mg^+NO complex may be qualitatively represented in C_s symmetry by the single-configuration wave function

$$[\text{core}](7a')^2(8a')^2(9a')^2(10a')^2(2a'')^2(11a')^2 \quad (1)$$

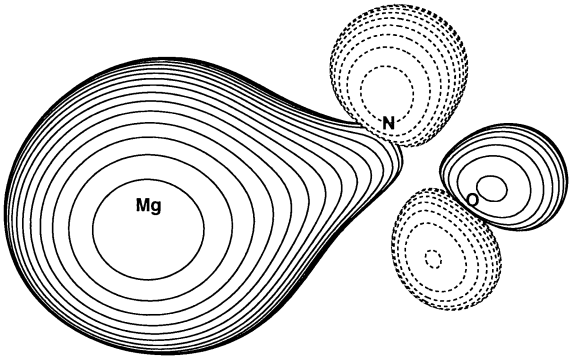

Fig. 1. Contour plot of the $^1A'$ Mg^+NO HOMO.

where [core] represents,

$$[\text{core}] = (1a')^2(2a')^2(3a')^2(4a')^2(5a')^2(1a'')^2(6a')^2 \quad (2)$$

Examination of contour plots of the SCF canonical and CISD natural orbitals provided a qualitative picture of the bonding. The valence orbitals, with the exception of the highest occupied molecular orbital (HOMO), were comprised of the NO σ, π, and nitrogen lone-pair orbitals. The HOMO, depicted in Fig. 1, exhibited the first visible evidence of bonding between the Mg and NO moieties; it consisted of a magnesium 3*s*-like orbital overlapping with a lobe of the in-plane NO π*-like orbital. The closed-shell $^1A'$ Mg^+ON complex exhibited similar bonding; the magnesium 3*s*-like orbital now interacts with a lobe situated on the oxygen terminus of the π*-like orbital (Fig. 2). However, the interaction in Mg^+ON was considerably weaker than in Mg^+NO, with no visible overlap, but a slight polarization of the orbitals toward

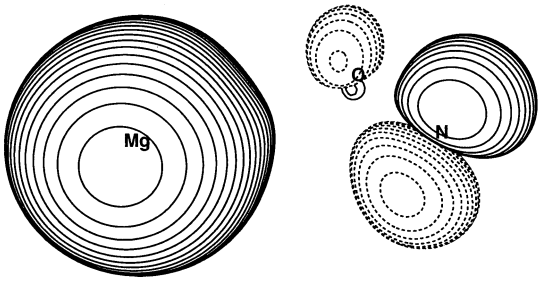

Fig. 2. Contour plot of the $^1A'$ Mg^+ON HOMO.

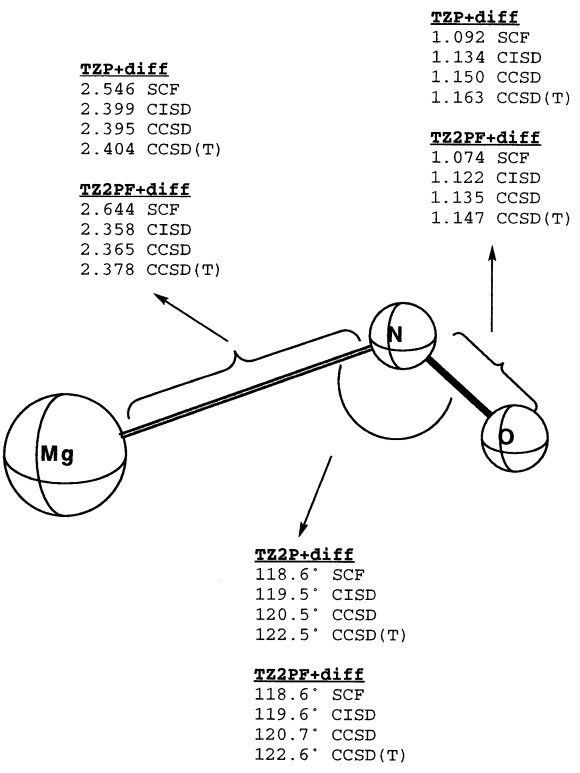

Fig. 3. Predicted equilibrium geometry of the closed-shell $^1A'$ state of Mg^+NO. Bond distances are in Å.

one another. Last, the single-configuration descriptions of $^1A'$ Mg^+ON and Mg^+NO differed primarily in that for Mg^+ON, the NO out-of-plane π orbital $(2a'')$ falls lower in energy than the nitrogen lone-pair orbital $(10a')$

$$[\text{core}](7a')^2(8a')^2(9a')^2(2a'')^2(10a')^2(11a')^2 \quad (3)$$

3.1.2. Equilibrium geometries

The predicted equilibrium geometries of the $^1A'$ Mg^+NO and Mg^+ON complexes are depicted in Figs. 3 and 4, respectively. In general, both complexes were strongly bent in accord with the picture of bonding occurring because of an interaction between a lobe of the NO π^* orbital and the Mg 3*s* orbital. The sole exceptions to this picture occurred for the more weakly bound $^1A'$ Mg^+ON complex at the TZP and TZP + diff CCSD(T) levels. At these two levels of theory the $^1A'$ Mg^+ON complex was no longer found to be a local minimum, however the addition of both higher angular momentum and polarization functions to the basis set, yielding the TZ2PF + diff basis set, removed the discrepancy and gave CCSD(T) results in agreement with the CISD and CCSD predictions.

With the TZ2PF + diff basis set, the largest used, successively more complete treatments of electron correlation resulted in a widening of the Mg^+NO bond angle, from the SCF prediction of 118.6° to the CCSD(T) prediction of 122.6°. The $^1A'$ Mg^+ON complex exhibited a similar trend with the bond angle increasing from 127.5° at the SCF level to 134.3° at the CCSD(T) level. With the same basis set, the Mg–N and Mg–O bond lengths were both observed to shorten as the electron correlation treatment was improved, whereas the NO bond lengths were found to elongate. Similar trends were observed with the two smaller basis sets.

3.1.3. Properties

Predictions of total energies, dipole moments, harmonic vibrational frequencies, and associated IR intensities for $^1A'$ Mg^+NO and Mg^+ON are provided in Tables 1 and 2, respectively. For the Mg^+NO complex, the NO stretch was predicted, within each basis set, to drop in frequency as the treatment of correlation effects became more complete. In contrast, the frequency of the Mg − N stretch was observed to increase. Relating the strength of a bond to both its length and stretching frequency, led to the conclusion that the addition of electron correlation weakened the NO bond, which became longer and decreased in stretching frequency, and strengthened the Mg–N bond, which became much shorter and increased in stretching frequency. For example, with the TZ2PF + diff basis set, the Mg–N bond length shrinks from 2.644 Å at the SCF level to 2.378 Å at the CCSD(T) level with a corresponding increase in the stretching frequency, from 123 cm^{-1} at the SCF level to 208 cm^{-1} at the CCSD(T) level. The same trend was observed to a much larger degree in the Mg^+ON structure. With the same basis set, the Mg–O bond shrinks from 3.497 Å at the SCF level to 2.332 Å at the CCSD(T) level with the corresponding increase in

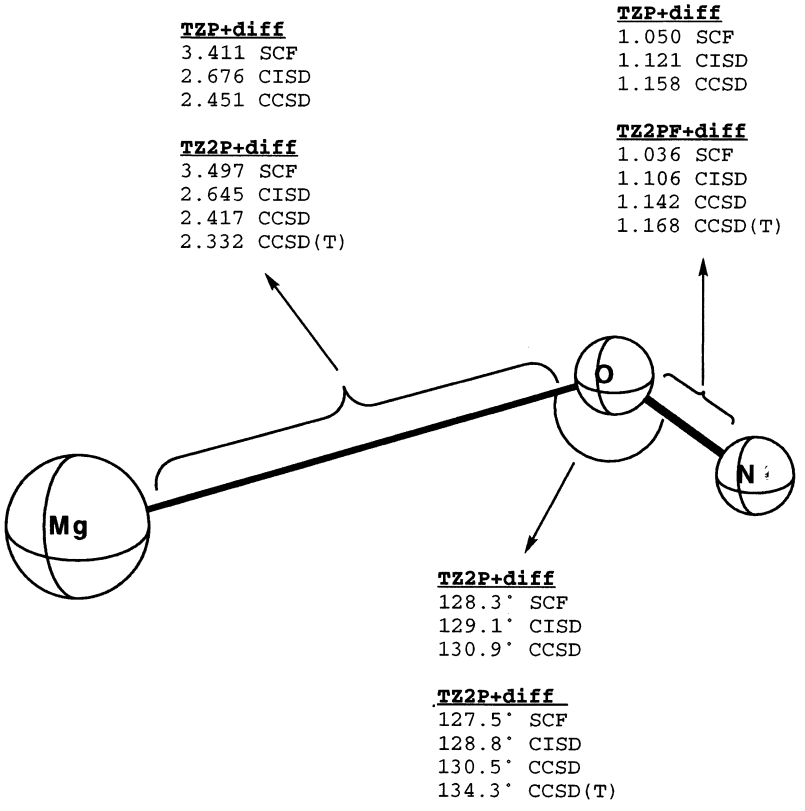

Fig. 4. Predicted equilibrium geometry of the closed-shell $^1A'$ state of Mg^+ON. Bond distances are in Å.

stretching frequency from 91 cm^{-1} at the SCF level to 101 cm^{-1} at the CCSD(T) level.

The change in the harmonic frequency of the NO stretching mode in the Mg^+NO and Mg^+ON complexes from the SCF to correlated levels was relatively large. The TZ2PF + diff SCF prediction for the NO stretching mode of the Mg^+ON complex was 2541 cm^{-1}, close to the experimental ω_e = 2376.42 cm^{-1} for isolated NO^+ [44], whereas the CISD, CCSD, and CCSD(T) predictions were all much closer to the experimental ω_e = 1904.2 cm^{-1} for neutral NO [44]. The SCF prediction appears to place more of the positive charge on NO rather than on Mg. Natural charges [45] at the TZ2PF + diff SCF level of theory were 0.17, 0.09, and 0.74 for Mg, O, and N, respectively. Furthermore, the TZ2PF + diff Mg^+ON SCF wave function predicted an NO bond length of 1.036 Å that is closer to the experimental r_e = 1.063 Å of NO^+ than the r_e = 1.151 Å of neutral NO [44]. On the other hand, the inclusion of correlation effects caused the positive charge to migrate onto the magnesium atom. The TZ2PF + diff CISD natural charges placed most of the positive charge on Mg and both the NO bond length of 1.106 Å and the NO stretching frequency of 1984 cm^{-1} were more closely in agreement with the neutral NO values. The migration of positive charge to the magnesium with the inclusion of correlation can be explained, in part, by the existence of a second important configuration

$$[\text{core}](7a')^2(8a')^2(9a')^2(10a')^2(2a'')^2(12a')^2 \quad (4)$$

in which the two electrons occupying the $11a'$ orbital are excited into the $12a'$ orbital, the lowest unoccupied molecular orbital (LUMO). The $12a'$ orbital,

Table 1
Total energies (Hartree), dipole moments (debye), harmonic vibrational frequencies (cm^{-1}), IR intensities (km mol^{-1}, in parentheses), and zero-point vibrational energies (ZPVE, in kcal mol^{-1}) for the closed shell $^1A'$ structure of Mg^+NO

Method	Energy	μ_e	ω_1 Mg − N stretch	ω_2 Bend	ω_3 N − O stretch	ZPVE
TZP SCF	− 328.59327	4.62	135 (106)	400 (62)	2143 (5484)	3.83
TZP + diff SCF	− 328.59389	4.77	134 (108)	402 (63)	2131 (5455)	3.81
TZP + diff CISD	− 329.04982	5.55	219 (7)	397 (31)	1965 (1866)	3.69
TZP + diff CCSD	− 329.16236	5.34	221 (3)	365 (20)	1879 (820)	3.52
TZP + diff CCSD(T)	− 329.19430	5.00	200 (13)	317 (21)	1802 (311)	3.32
TZ2P SCF	− 328.60245	3.76	122 (101)	391 (56)	2192 (5610)	3.87
TZ2P + diff SCF	− 328.60273	3.82	123 (102)	392 (56)	2189 (5608)	3.86
TZ2PF SCF	− 328.60807	3.74	123 (101)	389 (56)	2207 (5619)	3.89
TZ2PF + diff SCF	− 328.60840	3.80	123 (101)	390 (56)	2204 (5612)	3.88
TZ2PF + diff CISD	− 329.11505	5.66	227 (10)	402 (38)	1975 (2005)	3.72
TZ2PF + diff CCSD	− 329.23529	5.31	228 (2)	371 (24)	1910 (898)	3.59
TZ2PF + diff CCSD(T)	− 329.27105	4.89	208 (11)	325 (23)	1843 (342)	3.40

depicted in Fig. 5, is the antibonding counterpart of the HOMO and its inclusion into correlated wave functions serves to pull electron density away from the magnesium atom, making it more positive. The CI coefficients of the reference configuration and configuration 5 in the TZ2PF + diff CISD wave function were $C_0 = 0.939$ and $C_1 = -0.129$, respectively. The relative importance of these configurations changed little when CISD natural orbitals were used in the CISD. Furthermore, with the TZ2PF + diff basis set, the CCSD T_1 diagnostic [46–48] at the CCSD(T) geometry was 0.0244, indicating the validity of the single-reference coupled cluster treatment.

The situation was less clear for the Mg^+NO complex. At the TZ2PF + diff SCF level of theory, the natural charges placed more than half of the positive charge on the magnesium atom, but the NO stretching frequency of 2204 cm^{-1} and the NO bond length of 1.074 Å were in accord with the values for NO^+. Fortunately, the ambiguity disappeared upon inclusion of correlation effects. At the TZ2PF + diff CISD level, natural charges clearly placed the positive charge on the magnesium atom and both the NO bond length of 1.122 Å and the NO stretching frequency of 1975 cm^{-1} are in agreement with the values for neutral NO. Akin to $^1A'$ Mg^+ON, examination of the TZ2PF + diff CISD one-particle density matrix indicated the existence of a second important configuration involving a double excitation from the $11a'$ orbital to its antibonding counterpart, the $12a'$ orbital (Fig. 6). The CI coefficients were $C_0 = 0.941$ and $C_1 = -0.122$, and changed little upon performing

Table 2
Total energies (Hartree), dipole moment (debye), harmonic vibrational frequencies (cm^{-1}), IR intensities (km mol^{-1}, in parentheses), and zero-point vibrational energies (ZPVE, in kcal mol^{-1}) for the closed shell $^1A'$ structure of Mg^+ON

Method	Energy	μ_e	ω_1 Mg − O stretch	ω_2 Bend	ω_3 N − O stretch	ZPVE
TZP + diff SCF	− 328.57437	2.33	94 (46)	221 (8)	2471 (5811)	3.98
TZP + diff CISD	− 329.02359	3.71	128 (18)	339 (17)	1974 (2784)	3.49
TZP + diff CCSD	− 329.14324	4.82	174 (27)	304 (13)	1874 (94)	3.36
TZ2PF + diff SCF	− 328.59133	3.06	91 (43)	201 (8)	2541 (4954)	4.05
TZ2PF + diff CISD	− 329.08665	3.69	121 (26)	348 (19)	1984 (3153)	3.51
TZ2PF + diff CCSD	− 329.21403	4.74	179 (24)	312 (14)	1900 (130)	3.42
TZ2PF + diff CCSD(T)	− 329.25840	4.66	101 (13)	216 (3)	1596 (347)	2.73

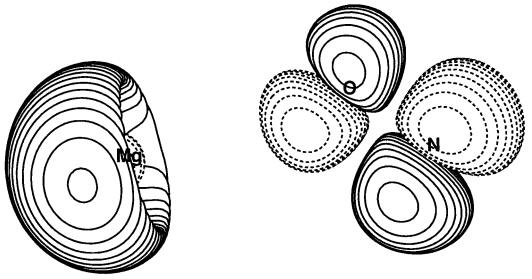

Fig. 5. Contour plot of the $^1A'$ Mg^+ON LUMO.

the CISD with natural orbitals from a prior CISD. With the TZ2PF + diff basis set, the CCSD T_1 diagnostic at the CCSD(T) geometry was 0.0213.

The change in the Mg^+NO and Mg^+ON charge distributions from the SCF wave function to correlated wave functions was also reflected in the dipole moments. In general, the dipole moments were large and suggest that both complexes might be observable using microwave spectroscopy. The dipole moment of $^1A'$ Mg^+NO was consistently predicted to be larger than that of $^1A'$ Mg^+ON. SCF predictions of the dipole moments were consistently lower than those predicted by correlated wave functions with the same basis set. The lower SCF dipole moments provided further evidence that the positive charge is not as localized in the SCF wave function and resides, in part, on the NO moiety. The CISD wave function always yielded a significant increase in the dipole moment over the SCF prediction. The increase in the dipole moment occurred in conjunction with the CISD wave function, moving most of the positive charge onto the magnesium atom. With the TZ2PF + diff basis set, the SCF prediction for the dipole moment of the Mg^+NO complex was 3.80 Debye (D), whereas the CISD prediction was 5.66 D, a difference of 1.86 D. For Mg^+ON the change was less drastic, going from 3.06 D to 3.69 D. More complete treatments of correlation beyond CISD caused the dipole moment of the Mg^+NO complex to drop, whereas the dipole moment of the Mg^+ON complex was first predicted to increase on going to the CCSD level of theory and then observed to decrease, slightly, with the addition of the (T) correction, CCSD(T).

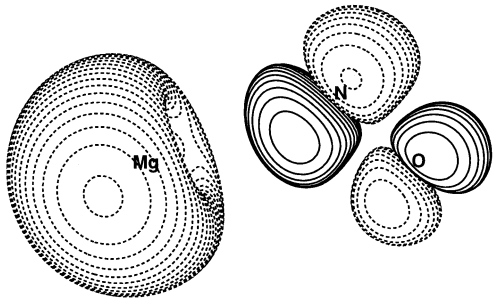

Fig. 6. Contour plot of the $^1A'$ Mg^+NO LUMO.

In addition to being highly sensitive to the completeness of the correlation treatment, predictions of the dipole moment were also extremely sensitive to the quality of the basis set. At the TZP SCF and TZP + diff SCF levels of theory, the dipole moment was predicted to be 4.62 D and 4.77 D respectively, whereas the TZ2PF + diff SCF wave function predicted a much lower dipole moment of 3.80 D. In order to confirm the TZ2PF + diff prediction of the dipole moment and examine the impact of the basis set on the SCF dipole moment prediction, SCF wave functions were constructed with three additional basis sets. The first basis set was constructed by removing the higher angular momentum functions from the TZ2PF + diff basis set, and was denoted TZ2P + diff. The second basis set, TZ2PF, consisted of the TZ2PF + diff basis set minus the diffuse functions. The third basis set removed both the higher angular momentum and the diffuse functions and was denoted TZ2P. The TZ2P, TZ2P + diff, and TZ2PF SCF predictions of the dipole moment were 3.76 D, 3.82 D, and 3.74 D, respectively, indicating that at the SCF level, the second set of polarization functions were primarily responsible for the lowering of the dipole moment prediction. The dipole moment predictions were much less sensitive to the basis set at correlated levels of theory. At the CISD level, the dipole moment increased by 0.17 D upon going from the TZP to the TZ2PF + diff basis set. The change in basis set sensitivity upon going from the SCF level to correlated levels may, in part, be attributed to the aforementioned delocalization of the positive charge at the SCF level.

3.2. $MgNO^+$ and $MgON^+$ charge–quadrupole complexes

While searching for the closed-shell complexes discussed in the previous section, two minima corresponding to $^1\Sigma^+$ $MgNO^+$ and $MgON^+$ charge–quadrupole complexes were discovered. Although not directly relevant to a study of Mg^+NO, these complexes lie on the $Mg - NO^+$ PES involved in the charge transfer reaction between neutral Mg and NO^+. Moreover, the interaction between Mg and NO^+ should be considerably weaker than that between Mg^+ and NO because of both the low polarizability of Mg and the delocalization of positive charge over the NO moiety. Therefore, it is likely that these charge–quadrupole complexes are the only low-lying minima on the $Mg - NO^+$ PES. Because aiding future investigation into the charge transfer mechanism is one of the goals of this project, TZ2PF + diff CCSD(T) predictions for the $^1\Sigma^+$ $MgNO^+$ and $MgON^+$ complexes are presented here.

The $^1\Sigma^+$ $Mg - NO^+$ charge–quadrupole complex was predicted to have Mg–N and N–O bond lengths of 3.961 Å and 1.068 Å, respectively. The NO bond length and harmonic stretching frequency of 2356 cm^{-1} are both in agreement with the experimental r_e = 1.063 Å and ω_e = 2376 cm^{-1} for isolated NO^+ [44]. The $Mg - N$ stretching frequency was predicted to be 75 cm^{-1}, whereas the doubly degenerate bending mode was predicted to have a frequency of 701 cm^{-1}. The $^1\Sigma^+$ $MgNO^+$ complex was predicted to lie 46.3 kcal mol^{-1} higher in energy than $^1A'$ Mg^+NO and 3.7 kcal mol^{-1} below the counterpoise [49,50] corrected $Mg + NO^+$ dissociation asymptote.

The analogous $^1\Sigma^+$ $MgON^+$ charge–quadrupole complex was predicted to have a Mg–O bond length of 3.82 Å, slightly shorter than the $Mg - N$ distance in the $MgNO^+$ complex. The NO bond length of 1.068 Å and the NO harmonic stretching frequency of 2363 cm^1 are close to the experimental r_e and ω_e of isolated NO^+. The $Mg - O$ stretching frequency and the doubly degenerate bending frequencies were determined to be 79 and 470 cm^{-1}, respectively. $^1\Sigma^+$ $Mg - ON^+$ was predicted to lie 38.0 kcal mol^{-1} higher in energy than $^1A'$ Mg^+ON and 45.9 kcal mol^{-1} higher than $^1A'$ Mg^+NO. The $Mg - ON^+$ complex was found to lie 4.1 kcal mol^{-1} below the counterpoise corrected $Mg + NO^+$ dissociation asymptote, and is therefore more strongly bound than the $Mg - NO^+$ complex, as was suggested by the higher $Mg - X$ (X = N or O) stretching frequency and the shorter Mg–X bond length.

3.3. The $^3\Pi$ structure of Mg^+NO and the $^3\Pi$ and $^3A'$ structures of Mg^+ON

3.3.1. Electronic structures

The $^3\Pi$ structure of the Mg^+NO complex may be represented in $C_{\infty v}$ symmetry by the single-configuration wave function

$$[\text{core}](6\sigma)^2(7\sigma)^2(8\sigma)^2(2\pi)^4(3\pi)(9\sigma) \quad (5)$$

where [core] represents,

$$[\text{core}] = (1\sigma)^2(2\sigma)^2(3\sigma)^2(4\sigma)^2(5\sigma)^2(1\pi)^4 \quad (6)$$

Examination of contour plots of the SCF canonical and CISD natural orbitals indicated that the 6σ, 7σ, 8σ, and 2π orbitals were two NO σ orbitals, a nitrogen lone-pair orbital, and a NO π orbital, respectively, with essentially no contribution from the magnesium atom. The singly occupied molecular orbitals (SOMOs), 3π and 9σ, may be described as an NO π^*-like orbital and as an antibonding interaction between a Mg 3*s*-like orbital and a nitrogen 2*p*-like orbital (Fig. 7), respectively. None of the occupied molecular orbitals exhibited visible overlap between Mg and NO orbitals, and when an interaction occurred, it was antibonding. The lack of $Mg - NO$ orbital overlap combined with the linear geometry suggest $^3\Pi$ Mg^+NO is essentially a charge–dipole complex. Furthermore, no bent minima were found on the triplet Mg^+NO PES, and the only stationary point observed was a transition state with a $Mg - N - O$ angle close to 90° corresponding to migration of the magnesium cation around the NO radical.

The situation was similar for $^3\Pi$ Mg^+ON, with the charge–dipole interaction occurring at the oxygen terminus of NO. The $^3\Pi$ state of Mg^+ON may be represented by the single-configuration wave function

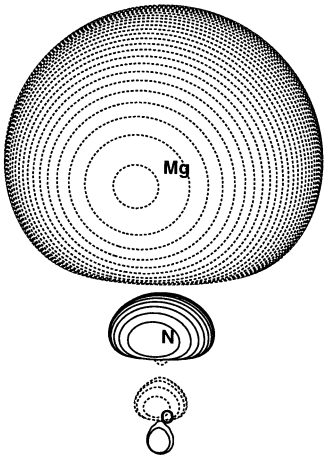

Fig. 7. Contour plot of the $^3\Pi$ Mg^+NO 9σ SOMO.

$$[\text{core}](6\sigma)^2(7\sigma)^2(2\pi_i)^2(8\sigma)^2(2\pi_o)^2(3\pi)(9\sigma) \quad (7)$$

that differs from Eq. (5) by a switch in the energetic ordering of the in-plane NO $2\pi_i$ orbital and the nitrogen lone-pair orbital, 8σ. Moreover, the 9σ SOMO (Fig. 8) is now an antibonding interaction between a Mg 3*s*-like orbital and an oxygen 2*p*-like orbital. At the TZP CISD, TZP CCSD, TZP CCSD(T), TZP + diff CCSD(T) levels of theory, the linear structure became a transition state between two bent C_s minima. The resulting $^3A'$ structures may be described by the single-configuration wave function

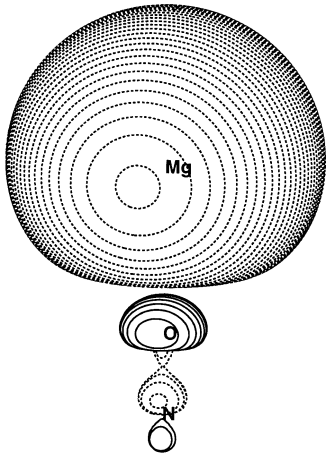

Fig. 8. Contour plot of the $^3\Pi$ Mg^+ON 9σ SOMO.

$$[\text{core}](7a')^2(8a')^2(9a')^2(10a')^2(2a'')^2(11a')(12a') \quad (8)$$

where [core] is given by Eq. (2).

3.3.2. Equilibrium geometries

The predicted equilibrium geometries of the $^3\Pi$ Mg^+NO and $^3\Pi$ Mg^+ON structures are provided together in Fig. 9. The NO bond lengths of the two complexes are all closer to the experimental r_e = 1.151 Å of neutral NO [44] than the shorter r_e = 1.063 Å of NO^+ [44]. Natural charges at the TZ2PF + diff SCF and CISD levels of theory support the conclusion that the positive charge is located on the magnesium. The addition of more complete treatments of correlation effects, within each basis set, caused the NO bond length to elongate in both the Mg^+NO and Mg^+ON complexes. In contrast, the Mg–N bond length shortened with improved correlation treatments, whereas the Mg–O bond length exhibited the opposite behavior. The addition of higher angular momentum functions and additional polarization functions to the basis set had a significant effect on the NO bond length. For $^3\Pi$ Mg^+NO, both the TZP and TZP + diff CCSD(T) wave functions predicted an NO bond length of 1.160 Å while the TZ2PF + diff basis set predicted a 1.144 Å NO bond length, 0.016 Å shorter.

The predicted equilibrium geometries of the $^3A'$ Mg^+ON structure, at the levels of theory and basis set where it is a minimum, are provided in Fig. 10. The shift of the Mg^+ON minimum between a linear and a bent geometry indicated the importance of large basis sets including diffuse and higher angular momentum functions, as well as high-level correlation methods including at least triple excitations, in providing an accurate description of the Mg^+ON complex. At the TZP CISD level, $^3A'$ Mg^+ON was predicted to have an NO bond length of 1.158 Å close to the value for neutral NO. More complete treatments of correlation for $^3A'$ Mg^+ON caused the NO bond length to elongate significantly, by 0.022 Å from TZP CISD to TZP CCSD(T). Natural charges at the TZP CISD level indicate that the positive charge is clearly on the

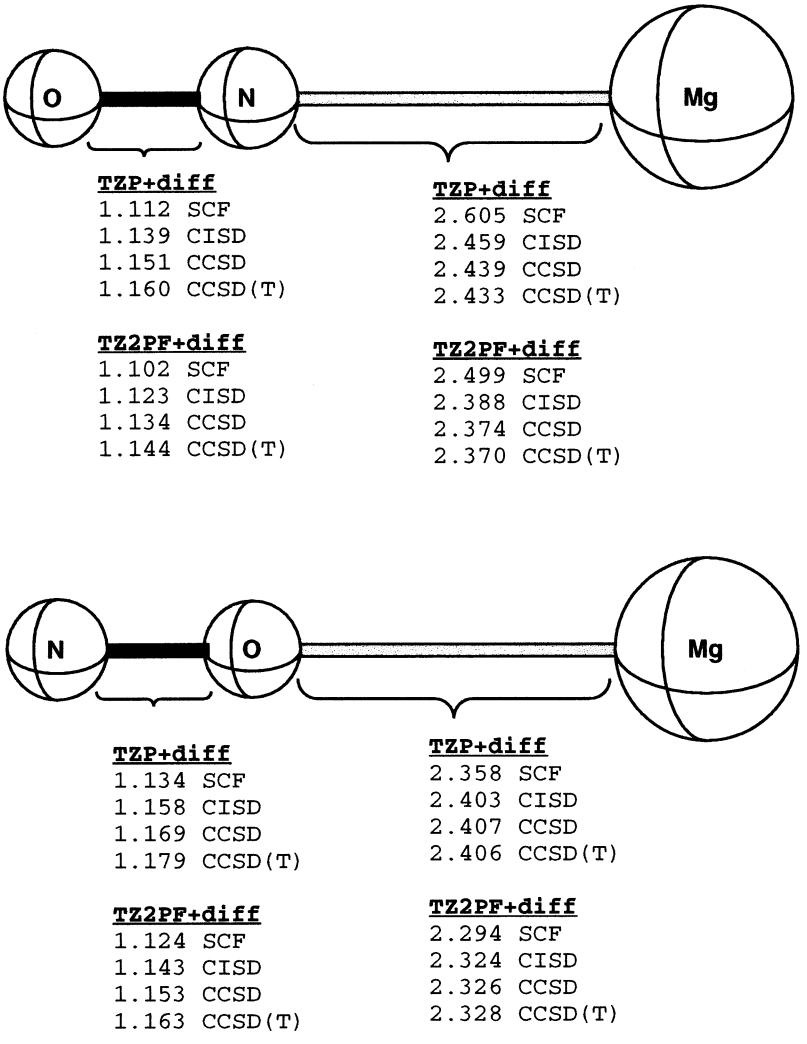

Fig. 9. Predicted equilibrium geometries for the $^3\Pi$ state of Mg^+NO and Mg^+ON. Bond distances are in Å.

magnesium. Thus, unlike the two closed-shell structures, the triplet structures never exhibited any ambiguity concerning the locus of positive charge; the charge is on the magnesium. The Mg–O bond in $^3A'$ Mg^+ON is relatively insensitive to the completeness of the correlated treatment: it elongated by only 0.004 Å from TZP CISD to TZP CCSD(T). However, it was affected by the addition of diffuse functions to the basis set; upon progressing from the TZP to the TZP + diff basis set the CCSD(T) prediction elongated by 0.015 Å.

3.3.3. Properties

Tables 3, 4, and 5 contain predictions of total electronic energies, dipole moments, harmonic vibrational frequencies, and associated IR intensities for the $^3\Pi$ Mg^+NO, $^3\Pi$ Mg^+ON, and $^3A'$ Mg^+ON structures, respectively. With the TZ2PF + diff basis set, $^3\Pi$ Mg^+NO exhibited an NO stretching frequency of 2344 cm^{-1} at the SCF level that decreased with more complete correlation treatments. At the TZ2PF + diff CCSD(T) level, the predicted NO stretching frequency of 1965 cm^{-1} was close to the

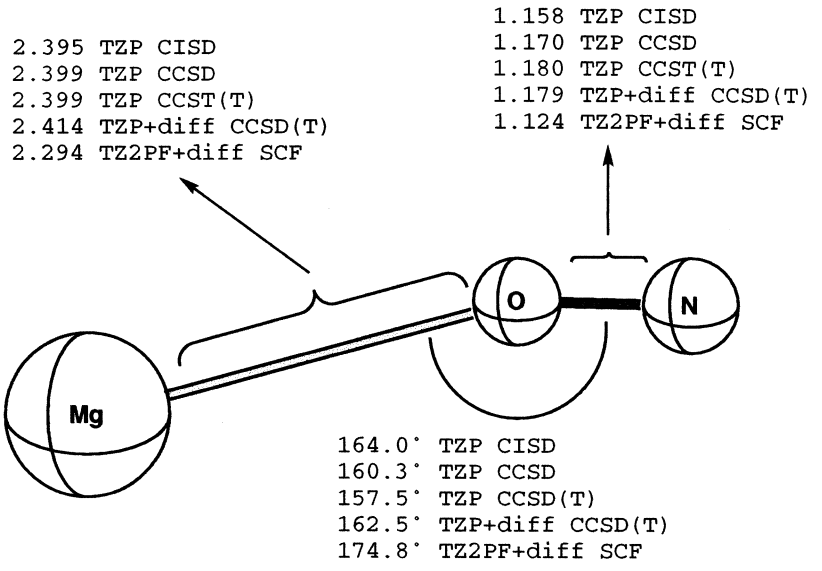

Fig. 10. Predicted equilibrium geometry for the $^3A'$ state of Mg^+ON. Bond distances are in Å.

experimental ω_e = 1904 cm^{-1} stretching frequency of neutral NO [44]. Whereas the NO bond decreased in frequency and elongated with improved correlation treatments, the Mg–N bond shortened and increased in stretching frequency, from 123 cm^{-1} at the TZ2PF + diff SCF to 186 cm^{-1} at the TZ2PF + diff CCSD(T) level. Similar trends in behavior were also exhibited with the two smaller basis sets, TZP and TZP + diff. The $^3\Pi$ state of Mg^+NO is doubly degenerate and was predicted to exhibit case A Renner–Teller splitting [51], i.e. the energies of the two components, although degenerate at the linear geometry, split upon bending, with one component increasing in energy faster than the other and therefore having a higher bending frequency. Taking the C_s plane of symmetry to be the plane of the 3π SOMO, the highest level of theory employed, TZ2PF + diff CCSD(T), predicted the A' and A'' components to have bending frequencies of 103 and 119 cm^{-1}, respectively.

As previously indicated, the triplet state of Mg^+ON is highly sensitive to both the basis set and

Table 3
Total energies (Hartree), dipole moment (debye), harmonic vibrational frequencies (cm^{-1}), IR intensities (km mol^{-1}, in parentheses), and zero-point vibrational energies (ZPVE, in kcal mol^{-1}) for the $^3\Pi$ structure of Mg^+NO

Method	Energy	μ_e	ω_1 Mg − N stretch	ω_2 N − O stretch	ω_3 A' component Bend[a]	ω_4 A'' component Bend[a]	ZPVE
TZP + diff SCF	− 328.65398	6.17	98 (91)	2323 (36)	67 (2)	147 (0)	3.77
TZP + diff CISD	− 329.07859	5.17	148 (95)	2126 (5)	70 (4)	141 (0)	3.55
TZP + diff CCSD	− 329.16905	5.01	159 (95)	2000 (2)	72 (4)	127 (0)	3.37
TZP + diff CCSD(T)	− 329.18549	4.96	163 (94)	1920 (1)	66 (4)	120 (0)	3.24
TZ2PF + diff SCF	− 328.66685	5.47	123 (96)	2344 (32)	79 (2)	157 (1)	3.86
TZ2PF + diff CISD	− 329.14468	4.70	172 (96)	2173 (5)	97 (3)	146 (1)	3.70
TZ2PF + diff CCSD	− 329.24302	4.59	182 (95)	2051 (2)	104 (3)	128 (1)	3.52
TZ2PF + diff CCSD(T)	− 329.26327	4.55	186 (95)	1965 (1)	103 (4)	119 (1)	3.39

[a] The C_s plane is taken to be the plane of the 3π SOMO.

Table 4
Total energies (Hartree), dipole moment (debye), harmonic vibrational frequencies (cm^{-1}), IR intensities (km mol^{-1}, in parentheses), and zero-point vibrational energies (ZPVE, in kcal mol^{-1}) for the $^3\Pi$ structure of Mg^+ON

Method	Energy	μ_e	ω_1 Mg − O stretch	ω_2 N − O stretch	ω_3 A' component Bend[a]	ω_4 A'' component Bend[a]	ZPVE
TZP + diff SCF	− 328.65771	4.46	132 (102)	2136 (332)	41 (6)	128 (2)	3.48
TZP + diff CISD	− 329.07606	5.08	127 (97)	1982 (200)	24 (4)	122 (1)	3.22
TZP + diff CCSD	− 329.16509	5.16	131 (97)	1884 (157)	3 (4)	117 (1)	3.05
TZP + diff CCSD(T)	− 329.18109	5.18	133 (96)	1799 (142)	23i (—)	113 (1)	2.92
TZ2PF + diff SCF	− 328.66930	4.11	152 (105)	2145 (322)	9i (—)	127 (1)	3.47
TZ2PF + diff CISD	− 329.14067	4.68	150 (101)	2020 (200)	36 (3)	120 (0)	3.32
TZ2PF + diff CCSD	− 329.23764	4.77	155 (100)	1923 (159)	47 (3)	114 (0)	3.20
TZ2PF + diff CCSD(T)	− 329.25736	4.81	157 (99)	1837 (141)	49 (3)	110 (0)	3.08

[a] The C_s plane is taken to be the plane of the 3π SOMO.

level of electron correlation. With the smallest basis set, TZP, the doubly degenerate $^3\Pi$ state was predicted to exhibit case A Renner–Teller splitting at the SCF level. Taking the C_s plane to be the plane of the 3π SOMO, an NO π^* orbital, the A' and A'' components of the $^3\pi$ state were predicted to possess bending frequencies of 25 and 125 cm^{-1}, respectively. With this same basis set, the CISD, CCSD, and CCSD(T) wave functions predicted the $^3\Pi$ state to exhibit case C Renner–Teller splitting [51] with the A' component possessing an imaginary bending frequency between 29 and 40 cm^{-1}. Following the imaginary mode led to the discovery of the $^3A'$ structure bent at roughly 160°. When a single set of diffuse functions was added to the TZP basis set, yielding the TZP + diff basis, the SCF, CISD, and CCSD wave functions predicted $^3\Pi$ Mg^+ON would exhibit Renner–Teller case A splitting with the bending mode of the A' component decreasing in frequency from 41 cm^{-1} at the SCF level to 3 cm^{-1} at the CCSD level, whereas the bending frequency of the A'' component went from 128 cm^{-1} at the SCF level to 117 cm^{-1} at the CCSD level. At the TZP + diff CCSD(T) level of theory, the frequency of the bending mode of the A' component became imaginary, once again indicating case C Renner–Teller splitting. With the largest basis set, TZ2PF + diff, the $^3\Pi$ Mg^+ON structure was predicted to be a local minimum displaying case A Renner–Teller splitting at the CISD, CCSD, and CCSD(T) levels of theory, but the SCF wave function predicted the A' component would have an imaginary bending frequency of 9 cm^{-1}.

The dipole moments of the $^3\Pi$ Mg^+NO and $^3\Pi$ Mg^+ON complexes were large: 4.55 D and 4.81 D, respectively, at the TZ2PF + diff CCSD(T) level of theory, and suggest that the two complexes might be observable via microwave spectroscopy. For both complexes, the dipole moment vector lies along the internuclear axis with the positive end located on the magnesium atom. Predictions of the dipole moments

Table 5
Total energies (Hartree), dipole moment (debye), harmonic vibrational frequencies (cm^{-1}), IR intensities (km mol^{-1}, in parentheses), and zero-point vibrational energies (ZPVE, in kcal mol^{-1}) for the $^3A'$ structure of Mg^+ON

Method	Energy	μ_e	ω_1 Mg − O stretch	ω_2 Mg − O − N bend	ω_3 N − O stretch	ZPVE
TZP CISD	− 329.07450	4.94	135 (97)	40 (4)	1980 (191)	3.08
TZP CCSD	− 329.16315	5.00	140 (96)	45 (3)	1880 (147)	2.95
TZP CCSD(T)	− 329.17904	5.00	143 (95)	50 (2)	1794 (131)	2.84
TZP + diff CCSD(T)	− 329.18110	5.16	131 (97)	103 (1)	1797 (125)	2.90
TZ2PF + diff SCF	− 328.66930	4.11	152 (105)	13 (4)	2145 (321)	3.28

Table 6
Relative energies (in kcal mol^{-1}) of the $^1A'$ and $^3\Pi$ states of $MgNO^+$, the $^1A'$, $^3\Pi$, and $^3A'$ states of $MgON^+$, and the $Mg^+ + NO$ dissociation asymptote

Level of theory	$^1A'$ Mg^+NO	$^1A'$ Mg^+ON	$^3\Pi$ Mg^+NO	$^3\Pi$ Mg^+ON	$^3A'$ Mg^+ON	$Mg^+ + NO$
TZP + diff SCF	0.00	12.2	− 37.7	− 40.0	—	− 34.6
TZP + diff CISD	0.00	16.5	− 18.1	− 16.5	—	—
TZP + diff CCSD	0.00	12.0	− 4.2	− 1.7	—	3.1
TZP + diff CCSD(T)	0.00	NA[a]	5.5	8.3	8.3	13.2
TZ2PF + diff SCF	0.00	10.7	− 36.7	− 38.2	—	− 32.9
TZ2PF + diff CISD	0.00	17.8	− 18.6	− 16.1	—	—
TZ2PF + diff CCSD	0.00	13.3	− 4.9	− 1.5	—	3.9
TZ2PF + diff CCSD(T)	0.00	7.9	4.9	8.6	—	14.1

[a] The $^1A'$ Mg^+ON complex was not a minimum at this level of theory.

of the two complexes exhibited opposite trends with respect to the completeness of the electron correlation treatment. With the TZ2PF + diff basis set, the total dipole moment of $^3\Pi$ Mg^+NO was observed to decrease with more complete correlation treatments, from 5.47 D at the SCF level to 4.55 D at the CCSD(T) level, whereas the dipole moment of the oxygen-bound $^3\Pi$ Mg^+ON was observed to increase from 4.11 D at the SCF level to 4.81 D at the CCSD(T) level. Similar trends in the dipole moment were seen with the two smaller basis sets.

3.3. Relative energies and dissociation energies

Relative energies of the $^1A'$ and $^3\Pi$ structures of Mg^+NO, the $^1A'$, $^3\Pi$, and $^3A'$ structures of Mg^+ON, and the $Mg + NO^+$ dissociation asymptote are provided in Table 6. The relative energetic ordering of the five structures was insensitive to the choice of basis set for a given correlated method. For the CISD and CCSD methods, the relative ordering was

$$^3\Pi\ MgNO^+ < {}^3A'\ MgON^+ < {}^3\Pi\ MgON^+ < {}^1A'\ MgNO^+ < {}^1A'MgON^+ \quad (9)$$

whereas for the CCSD(T) method, $^1A'$ Mg^+NO dropped significantly in energy and became the global minimum

$$^1A'Mg\ NO^+ < {}^3\Pi\ MgNO^+ < {}^3A'\ MgON^+ < {}^3\Pi\ MgON^+ < {}^1A'\ MgON^+ \quad (10)$$

Within a given basis set, the energy difference between $^3\Pi$ Mg^+NO and $^1A'$ Mg^+NO dropped significantly upon inclusion of more complete correlation treatments. With the TZ2PF + diff basis set, the SCF wave function predicted an energy difference of 36.7 kcal mol^{-1}; the CISD wave function a difference of 18.6 kcal mol^{-1} (roughly half the SCF prediction); the CCSD wave function a difference of 4.9 kcal mol^{-1} (about one-quarter of the CISD prediction), and the CCSD(T) method predicted $^1A'$ Mg^+NO to lie 4.9 kcal mol^{-1} below $^3\Pi$ Mg^+NO. The large changes in the relative energies of these two structures demonstrated the importance of more complete correlation treatments in providing an accurate determination of the global minimum and relative energetics of the $Mg^+ - NO$ complex. The size of the basis set was less important; the TZP basis set predicted the same energetic ordering of the structures as the TZ2PF + diff basis set and differed from the TZ2PF + diff predictions for a given method by less than 3 kcal mol^{-1}. However, at the SCF level, the choice of basis set was important in determining the relative energies of the $^3\Pi$ Mg^+NO and $^3\Pi$ Mg^+ON structures. The $^3\Pi$ state of Mg^+ON was predicted to be the global minimum by the TZP and TZ2PF + diff SCF wave functions, whereas $^3\Pi$ Mg^+NO was predicted to be the global minimum by the TZP + diff SCF wave function.

The last column in Table 6 provides the relative energy of the $Mg^+ + NO$ dissociation asymptote with respect to $^1A'$ Mg^+NO, the global minimum at

the CCSD(T) level of theory. The energy of the $Mg^+ + NO$ asymptote was determined at the CCSD and CCSD(T) levels because these methods are size consistent, allowing the energy of the two fragments to be computed separately and added together, and it had already been demonstrated that highly correlated treatments were necessary to yield accurate relative energies. With the largest basis set, TZ2PF + diff, the $Mg^+ + NO$ asymptote was predicted to lie 3.89 and 14.07 kcal mol^{-1} above $^1A'$ Mg^+NO at the CCSD and CCSD(T) levels of theory, respectively.

4. Conclusions

In order to aid future research into the charge transfer reaction between Mg and NO^+, a reaction proposed to be of importance in the formation of Mg^+ in the ionosphere, the $Mg^+ - NO$ complex was examined using high level ab initio electronic structure methods. Equilibrium geometries, dipole moments, harmonic vibrational frequencies, and associated IR intensities were provided for the lowest triplet and singlet structures of Mg^+NO and Mg^+ON. At the highest level of theory employed, TZ2PF + diff CCSD(T), the $^1A'$ Mg^+NO structure was predicted to be the global minimum, lying 14 kcal mol^{-1} below the $Mg^+ + NO$ dissociation asymptote. The Mg–N bond in $^1A'$ Mg^+NO was observed to involve, in part, a covalent interaction between a Mg 3*s*-like orbital and a NO π^* orbital, explaining the preference for a bent structure over the linear geometry expected for a typical charge–dipole interaction. Correlation effects were found to be very important in describing this complex. With the TZ2P + diff basis set, the SCF wave function $^1A'$ Mg^+NO was predicted to lie 40 kcal mol^{-1} above the linear $^3\Pi$ Mg^+NO and Mg^+ON structures, but increasingly more complete treatments of correlation effects lowered the energy of $^1A'$ Mg^+NO relative to $^3\Pi$ Mg^+NO, until it became the global minimum at the CCSD(T) level.

Acknowledgements

This research was supported by the U.S. National Science Foundation, Grant CHE-9527468. The authors would like to thank Professor Michael A. Duncan for suggesting this project and providing many helpful discussions. BCH would also like to thank Dr. T.D. Crawford, Dr. W.D. Allen, and Dr. Yukio Yamaguchi for helpful discussions and insights.

References

[1] J.M.C. Plane, Int. Rev. Phys. Chem. 10 (1991) 55.
[2] J. Gardner, R.A. Viereck, E. Murad, S.T. Lai, D. Knecht, L. Broadfoot, E. Anderson, W. Sandel, W.J. McNeil, Proc. SPIE Int. Soc. Opt. Eng. 2266 (1994) 262.
[3] J. Gardner, R.A. Viereck, E. Murad, D. Knecht, C.P. Pike, L. Broadfoot, E.R. Anderson, Geophys. Res. Lett. 22 (1995) 2119.
[4] W.J. McNeil, S.T. Lai, E. Murad, J. Geophys. Res. 101 (1996) 5251.
[5] K.F. Willey, C.S. Yeh, D.L. Robbins, J.S. Pilgrim, M.A. Duncan, J. Chem. Phys. 97 (1992) 8886.
[6] C.S. Yeh, K.F. Willey, D.L. Robbins, J.S. Pilgrim, M.A. Duncan, J. Chem. Phys. 98 (1993) 1867.
[7] L.N. Ding, M.A. Young, P.D. Kleiber, W.C. Stwalley, A.M. Lyyra, J. Phys. Chem. 97 (1993) 2181.
[8] C.S. Yeh, J.S. Pilgrim, K.F. Willey, D.L. Robbins, M.A. Duncan, Int. Rev. Phys. Chem. 13 (1994) 231.
[9] J.S. Pilgrim, C.S. Yeh, K.R. Berry, M.A. Duncan, J. Chem. Phys. 100 (1994) 7945.
[10] R.J.L. Roy, J. Chem. Phys. 101 (1994) 10 217.
[11] D.L. Robbins, L.R. Brock, J.S. Pilgrim, M.A. Duncan, J. Chem. Phys. 102 (1995) 1481.
[12] C.T. Scurlock, J.S. Pilgrim, M.A. Duncan, J. Chem. Phys. 103 (1995) 3293.
[13] S. Matsika, R.M. Pitzer, J. Phys. Chem. 102 (1998) 1652.
[14] C.W. Bauschlicher, H. Partridge, S.R. Langhoff, J. Chem. Phys. 91 (1989) 4733.
[15] C.W. Bauschlicher, H. Partridge, S.R. Langhoff, Chem. Phys. Lett. 165 (1990) 272.
[16] C.W. Bauschlicher, H. Partridge, Chem. Phys. Lett. 181 (1991) 129.
[17] C.W. Bauschlicher, H. Partridge, J. Phys. Chem. 95 (1991) 3946.
[18] H. Partridge, C.W. Bauschlicher, S.R. Langhoff, J. Phys. Chem. 96 (1992) 5350.
[19] C.W. Bauschlicher, M. Sodupe, H. Partridge, J. Chem. Phys. 96 (1992) 4453.
[20] M. Sodupe, C.W. Bauschlicher, H. Partridge, Chem. Phys. Lett. 192 (1992) 185.
[21] M. Sodupe, C.W. Bauschlicher, Chem. Phys. Lett. 195 (1992) 494.
[22] C.W. Bauschlicher, Chem. Phys. Lett. 201 (1993) 11.
[23] C.W. Bauschlicher, M. Sodupe, Chem. Phys. Lett. 214 (1993) 489.

[24] C.W. Bauschlicher, H. Partridge, Chem. Phys. Lett. 239 (1995) 241.
[25] A.D. McLean, G.S. Chandler, J. Chem. Phys. 72 (1980) 5639.
[26] S. Huzinaga, J. Chem. Phys. 42 (1965) 1293.
[27] T.H. Dunning, J. Chem. Phys. 55 (1971) 716.
[28] P. Pulay, Mol. Phys. 17 (1969) 197.
[29] J.D. Goddard, N.C. Handy, H.F. Schaefer, J. Chem. Phys. 71 (1979) 1525.
[30] B.R. Brooks, W.D. Laidig, P. Saxe, J.D. Goddard, Y. Yamaguchi, H.F. Schaefer, J. Chem. Phys. 72 (1980) 4652.
[31] Y. Osamura, Y. Yamaguchi, H.F. Schaefer, J. Chem. Phys. 75 (1981) 2919.
[32] Y. Osamura, Y. Yamaguchi, H.F. Schaefer, J. Chem. Phys. 77 (1982) 383.
[33] J.E. Rice, R.D. Amos, N.C. Handy, T.J. Lee, H.F. Schaefer, J. Chem. Phys. 85 (1986) 963.
[34] G.D. Purvis, R.J. Bartlett, J. Chem. Phys. 76 (1982) 1910.
[35] M. Rittby, R.J. Bartlett, J. Phys. Chem. 92 (1988) 3033.
[36] J. Gauss, W.J. Lauderdale, J.F. Stanton, J.D. Watts, R.J. Bartlett, Chem. Phys. Lett. 182 (1991) 207.
[37] J.D. Watts, J. Gauss, R.J. Bartlett, Chem. Phys. Lett. 200 (1992) 1.
[38] J.D. Watts, J. Gauss, R.J. Bartlett, J. Chem. Phys. 98 (1993) 8717.
[39] J.A. Pople, R. Krishnan, H.B. Schlegel, J.S. Binkley, Int. J. Quantum Chem., Quantum Chem. Symp. 13 (1979) 225.
[40] P. Saxe, Y. Yamaguchi, H.F. Schaefer, J. Chem. Phys. 77 (1982) 5647.
[41] Y. Osamura, Y. Yamaguchi, P. Saxe, M.A. Vincent, J.F. Gaw, H.F. Schaefer, Chem. Phys. 72 (1982) 131.
[42] C.L. Janssen, E.T. Seidl, G.E. Scuseria, T.P. Hamilton, Y. Yamaguchi, R.B. Remington, Y. Xie, G. Vacek, C.D. Sherrill, T.D. Crawford, J.T. Fermann, W.D. Allen, B.R. Brooks, G.B. Fitzgerald, D.J. Fox, J.F. Gaw, N.C. Handy, W.D. Laidig, T.J. Lee, R.M. Pitzer, J.E. Rice, P. Saxe, A.C. Scheiner, H.F. Schaefer, PSI 2.0.8, PSITECH, Inc., Watkinsville, GA 30677, USA, 1995. This program is generally available without charge via the Internet.
[43] J.F. Stanton, J. Gauss, W.J. Lauderdale, J.D. Watts, R.J. Bartlett, ACES II. The package also contains modified versions of the MOLECULE Gaussian integral program by J. Almlöf and P.R. Taylor; the ABACUS integral derivative program written by T.U. Helgaker, H.J.Aa. Jensen, P. Jørgensen, and P.R. Taylor; and the PROPS property evaluation integral code by P.R. Taylor.
[44] K.P. Huber, G. Herzberg, Constants of Diatomic Molecules, Van Nostrand Reinhold, New York, 1979.
[45] A.E. Reed, L.A. Curtiss, F. Weinhold, Chem. Rev. 88 (1988) 899.
[46] T.J. Lee, J.E. Rice, G.E. Scuseria, H.F. Schaefer, Theor. Chim. Acta 75 (1989) 81.
[47] T.J. Lee, P.R. Taylor, Int. J. Quantum Chem., Quantum. Chem. Symp. 23 (1989) 199.
[48] D. Jayatilaka, T.J. Lee, J. Chem. Phys. 98 (1993) 9734.
[49] H.B. Jansen, P. Ros, Chem. Phys. Lett. 3 (1969) 140.
[50] S.F. Boys, F. Bernardi, Mol. Phys. 19 (1970) 553.
[51] T.J. Lee, D.J. Fox, H.F. Schaefer, R.M. Pitzer, J. Chem. Phys. 81 (1984) 356.